

TESTS OF JOINTS IN AAC MASONRY WALLS

Iwona GALMAN^a, Radosław JASIŃSKI^b

^a PhD; Department of Structural Engineering, Silesian University of Technology, Akademicka 5, 44-100 Gliwice, Poland
E-mail address: iwona.galman@polsl.pl

^b Phd DSc Prof.; Department of Building Structures, Silesian University of Technology, Akademicka 5, 44-100 Gliwice, Poland
E-mail address: radoslaw.jasinski@polsl.pl

Received: 21.05.2018; Revised: 9.10.2018; Accepted: 6.11.2018

Abstract

The paper presents the results of the Authors' tests on the joints in AAC masonry walls. The shape of the tested element and the test stand were fitted innovatively based on the Authors' own experience as well as on the literature overview and numerical analysis. Cracking morphology and mode of failure were investigated. The relationship between the load and displacement for different types of joints was compared. The obtained results were also compared to the results obtained on the reference model, which was a model with a traditional masonry bond. In the remaining testing elements, the connection was realized with the use of steel connectors. Various mechanisms of cracking and failure have been observed as well as the behaviour and load-bearing capacity of joints were different. The obtained results encourage to further analyses focused on detailing the joints and application of new methods in the construction of the joints.

Keywords: Masonry structures; Stiffening walls; Wall joints; Connectors; Bed joint reinforcement.

1. INTRODUCTION

The overview of laboratory tests of joints presented in [1] shows that there are no complete works related to the investigation of the behaviour of wall joints. This concerns not only walls made of AAC blocks but also the walls made of other masonry units. Because the problem of joints and co-operation between the walls is poorly investigated, calculations of such structures are hardly made. There are no code regulations for determination of internal forces and stresses acting in the intersection of the walls as well as for ULS and SLS control. A few existing tests do not allow to describe the mechanism of work of a wall joint, let alone to formulate the rules for design or construction. Therefore, the authors defined the following goals of their research:

- To investigate the mechanism of cracking and failure of the walls made of AAC blocks (most popular masonry units currently used in Poland),

- To compare the load-bearing capacity of wall joints made with traditional masonry bond and with the use of steel connectors,
- To aim at formulating simplified models of the behaviour of unreinforced and reinforced wall joints.

2. OWN RESEARCH PROGRAM

In the pilot tests where the models were composed of a web wall and two perpendicular flange walls, the obtained results were difficult to interpret and it was impossible to evaluate the behaviour of a single joint. To avoid this drawback, in the main phase of the tests the shape of the test elements and the test stand were changed. The tests were performed in the dedicated, specifically designed test stand, composed of a steel frame and vertical confining elements. The force causing shear in the joint was induced by a hydraulic jack

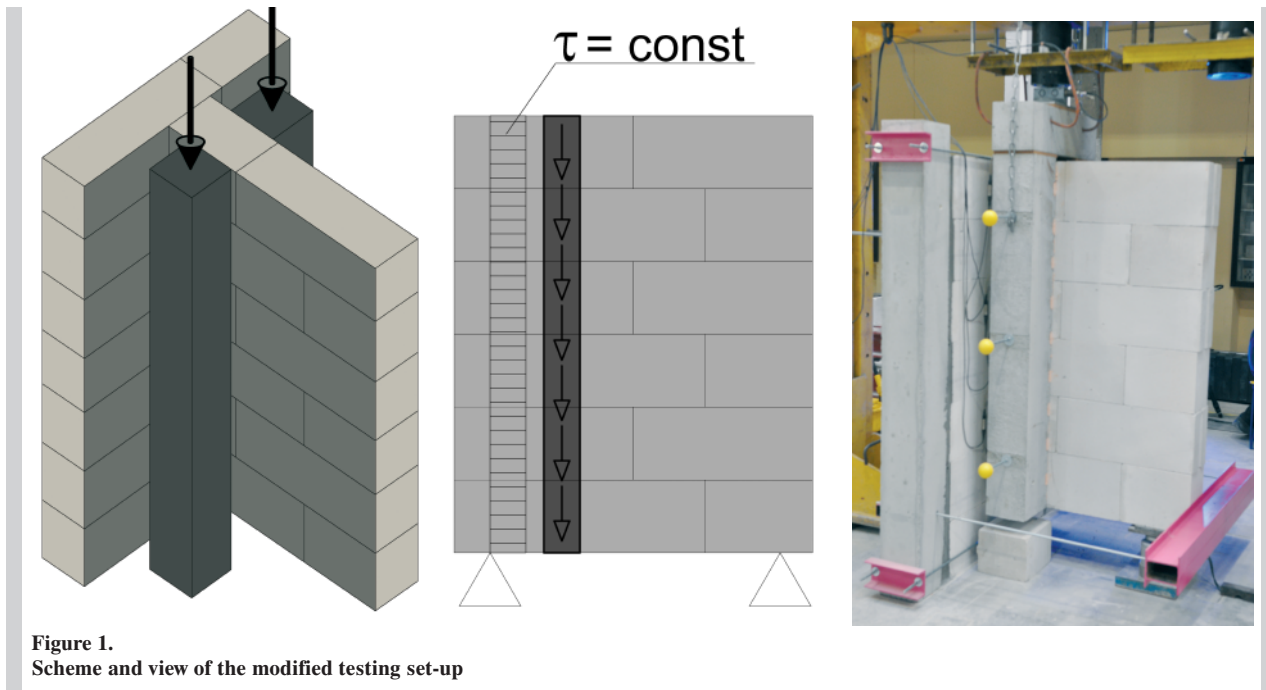


Figure 1.
Scheme and view of the modified testing set-up

of 1000 kN range and measurements were recorded with a force gauge of 250 kN range. The models were loaded in one cycle until failure by applying the force with 0.1 kN/s speed. The distance between the supports was equal to 87 cm. Vertical load generating shear was transferred linearly along the whole height of the wall; thanks to that uniform shear stress was induced in the joint. Static scheme of the test models and the view of the test stand are shown in Fig. 1. During the test continuous recordings were made of the loading and displacement of the loaded wall with respect to the non-loaded wall. Recordings were made with two independent systems. One side of the test model was monitored with the use of the optical displacement recorder ARAMIS. The other side was monitored with the use of three inductive displacement transducers of PJX-10 type with 10 mm range and 0.002 mm accuracy.

The tests were performed on the models made of AAC masonry units and system mortar for thin joints, with unfilled head joints. Compressive strength of masonry, determined acc. to PN-EN 1052-1:2000 and presented in [2], was equal to $f_c = 2.97 \text{ N/mm}^2$, modulus of elasticity was equal to $E_m = 2040 \text{ N/mm}^2$, initial shear strength, determined acc. to PN-EN 1052-3:2004 and presented in [3] was equal to $f_{vo} = 0.31 \text{ N/mm}^2$, and shear modulus, determined acc. to ASTM E519-81 and presented in [4] was equal to $G = 329 \text{ N/mm}^2$.

Three series of three models of identical shape and size were made and tested. The models were monosymmetric and had a T shape with a web and a flange of $\sim 89 \text{ cm}$ length. A joint was formed between the loaded and non-loaded wall, which structure was differentiated. In the series of models denoted as **P**, a traditional masonry bond was made between the web and the flange (Fig. 2a). These were the reference elements which mechanical parameters and behaviour during loading and failure were compared with the results of other tests. In the next two series of walls (geometry acc. to Fig. 2b) the joint between the walls was realised with the use of steel connectors, with no bond of masonry units. In the elements of **B** series, the joint was formed by immersing horizontal single punched flat profiles in bed joints (Fig. 2c). In the elements of **F** series $\phi 10$ steel bars of 36 cm length were applied, anchored in each layer of masonry units (Fig. 2d). Bars were placed into the previously drilled holes across the whole thickness of the flange wall and anchored by 18 cm in the web wall. The bars were additionally stabilised with PUR foam. The names of the elements with the shapes of connectors as well as their geometrical and mechanical parameters are collectively presented in Table 1.

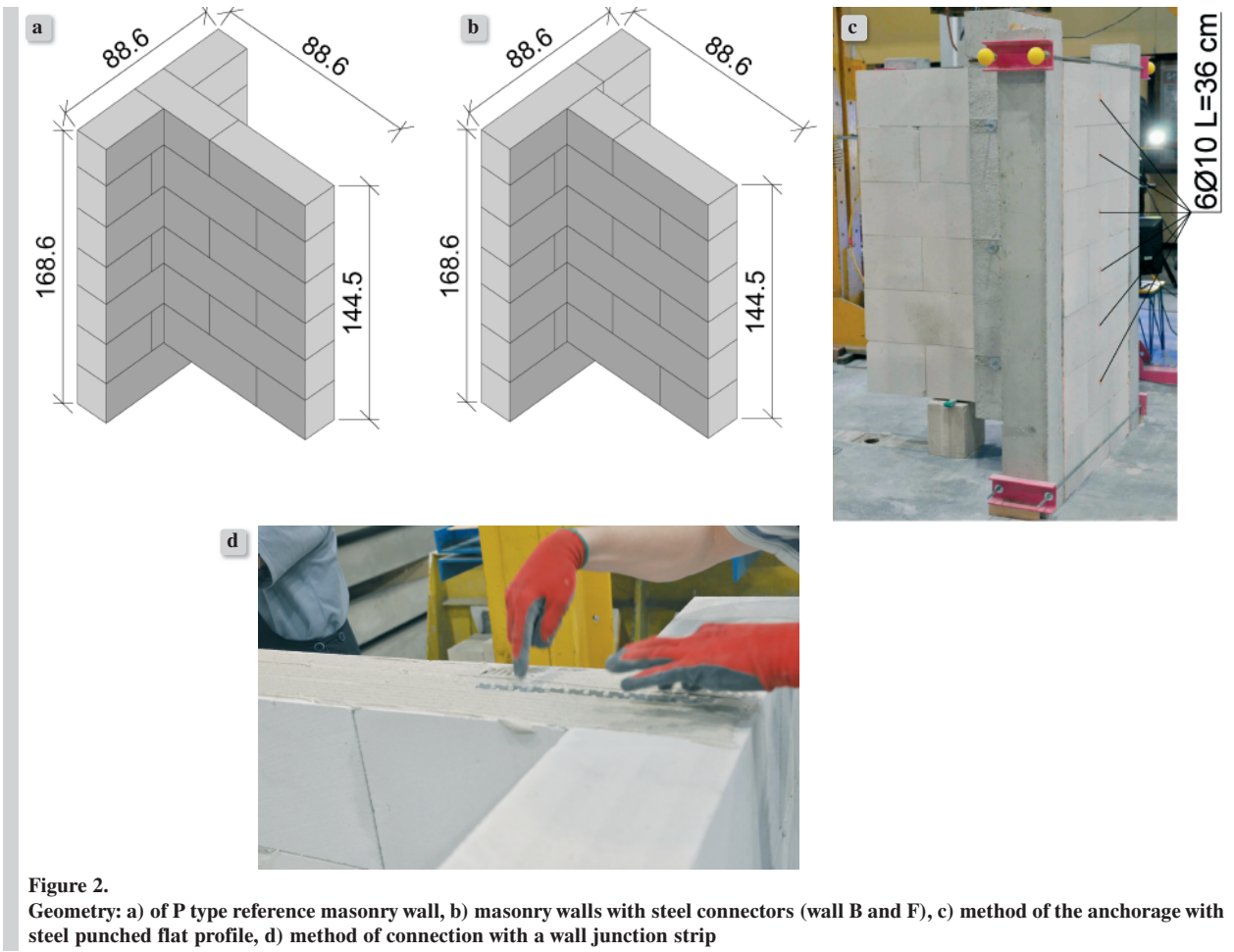




Figure 2. Geometry: a) of P type reference masonry wall, b) masonry walls with steel connectors (wall B and F), c) method of the anchorage with steel punched flat profile, d) method of connection with a wall junction strip

Table 1. Testing program

Series name	Type of joint	l mm	A mm ²	I mm ⁴	f_y N/mm ²	E_s N/mm ²	No. of walls in series
P	Traditional masonry bond	--	--	--	--	--	3
B	Perforated wall junction strip $b \times t = 22 \times 1$ mm 	300 (300 t)	22	1.83	144	66225	3
F	Steel bar $\phi 10$ 	300 (30 ϕ)	79	491	536	190500	3

l – connector's length, A – cross-sectional area, I – a moment of inertia, f_y – average yield strength steel, E_s – modulus of elasticity steel



Figure 3. Failure of a P series model a) first cracks in the reference model P_2 b) view of the joint at the moment of failure P_3

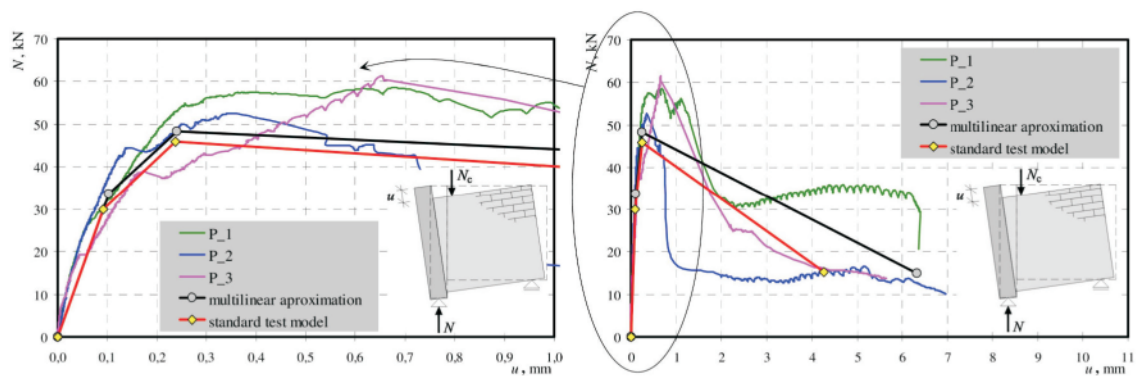


Figure 4. Relationship between the total force and mean relative displacement of the joint – test and calculation results

3. TEST RESULTS AND ANALYSIS

3.1. Unreinforced models

All the tested unreinforced models behaved in a similar manner. In the initial phase of loading, no crashes were heard and no spalling of side surfaces of the elements were visible. This phase lasted until first slanted cracks appeared in the direct vicinity of the joint (Fig. 3a). The increase of loading caused significant development of cracks at the joint and their propagation towards the reinforced concrete column transferring the load. The high-est value of force was

registered in this phase. Further loading caused an important increase of relative displacements and rotation of the joined walls. After the failure the joint was dismantled (Fig. 3b) which revealed almost vertical shearing of the elements in the joint. No visible damages were noticed in other elements.

Mechanism of cracking of the elements is also visible in the diagrams of the relationship between the load N and the relative displacement u of the joined walls (Fig. 4). Force N was taken as a difference between the load (induced force) and support reaction. Before

Table 2.
Test results

Model	Cracking force		Force at failure		Residual force		Displacement at the moment of cracking		Displacement right before failure		Residual displacement	
	N_{cr} kN	$N_{cr,mv}$ kN	N_u kN	$N_{u,mv}$ kN	N_r kN	$N_{r,mv}$ kN	u_{cr} mm	$u_{cr,mv}$ mm	u_u mm	$u_{u,mv}$ mm	u_r mm	$u_{r,mv}$ mm
P_1	27.3	33.7	56.3	48.3	20.7	14.9	0.07	0.10	0.31	0.24	6.36	6.32
P_2	42.6		50.0		10.2		0.12		0.25		6.97	
P_3	31.2		38.6		13.8		0.12		0.16		5.64	

cracking of the joint, which occurred under the level of load of $N_{cr} = 27.3\text{--}42.6$ kN, displacements increased almost proportionally, and this phase was referred to as an elastic phase. After cracking, in the post-elastic phase reduction of stiffness was observed, but the joints were still able to transfer the load.

This phase finished under the maximum forces of $N_u = 38.6\text{--}56.3$ kN. Further loading in the failure phase caused a visible decrease of forces registered by the strength meter, accompanied with an increase of relative displacements. Forces did not drop to zero and the joint was able to transfer some load. In the final phase, hard-ening was observed – an increase of the registered force. The last registered forces, tentatively called residua forces, preceded failure which was connected with the complete loosening of the joined elements and their rotation and were equal to $N_r = 10.2\text{--}18.8$ kN. The values of forces and corresponding displacements are collectively presented in Table 2, while linear approximation is shown in Fig. 5. In each phase of work stiffnesses of the joints were determined according to the Eqs. (1–3) and collectively presented in Table 3:

- elastic joint stiffness:

$$K_t = \frac{N_{cr}}{u_{cr}}, \quad (1)$$

- post-elastic joint stiffness:

$$K_p = \frac{N_u - N_{cr}}{u_u - u_{cr}}, \quad (2)$$

- residual joint stiffness:

$$K_r = \frac{|N_r - N_u|}{u_r - u_u}. \quad (3)$$

Based on the performed test an attempt was made to describe the work of the unreinforced wall joint analytically. The following assumptions were made:

- walls are made of the Group 1 elements without holes with thin joints and unfilled head joints,
- thickness of the stiffening wall is not bigger than the thickness of the transverse wall,

Table 3.
Joint stiffness

Model	Elastic joint stiffness		Residual joint stiffness		Residual force	
	K_t MN/m	$K_{t,mv}$ MN/m	K_p MN/m	$K_{p,mv}$ MN/m	K_r MN/m	$K_{r,mv}$ MN/m
P_1	413	341	119	114	6	5
P_2	341		60		6	
P_3	268		163		5	

d) there are two phases of work of the wall joint: elastic, post-elastic and failure,

- Elastic phase in the range of loads $0 - N_{cr}$ and displacements $0 - u_{cr}$,
- Post-elastic phase in the range of loads $N_{cr} - N_u$ and displacements $u_{cr} - u_u$,
- Failure phase in the range of loads $N_u - N_r$ and displacements $u_u - u_r$,

in which the relationships between the load and displacement $N - u$ are approximated with straight lines. A conceptual scheme of joint's work is shown in Fig. 5 while the comparison between the tests and calculation results are shown collectively in Table 4. In [5] the authors presented a simplified empirical model for determination of mechanical parameters of the joints based on the standard code tests performed according to ASTM E519-81 [3] and PN-EN 1052-3:2004 [4]. The form of the functions describing the work of the joint in each phase was defined with the following relationships:

- elastic joint stiffness and displacement:

$$K_t = \alpha K_{RL} \Rightarrow u_{cr} = N_{cr} / K_t, \quad (4)$$

$$N_{cr} = \alpha_1 \tau_{cr,RL} A, \quad (5)$$

- post-elastic joint stiffness:

$$K_p = \beta K_t \Rightarrow u_u = u_{cr} + (N_u - N_{cr}) / K_p, \quad (6)$$

$$N_u = \beta_1 \tau_{u,RL} A, \quad (7)$$

where: $A = 0.26 \text{ m}^2$ – area of the joint, $\alpha = 2.8$, $\alpha_1 = 0.6$, $\beta = 0.33$, $\beta_1 = 0.9$ – empirical coefficients.

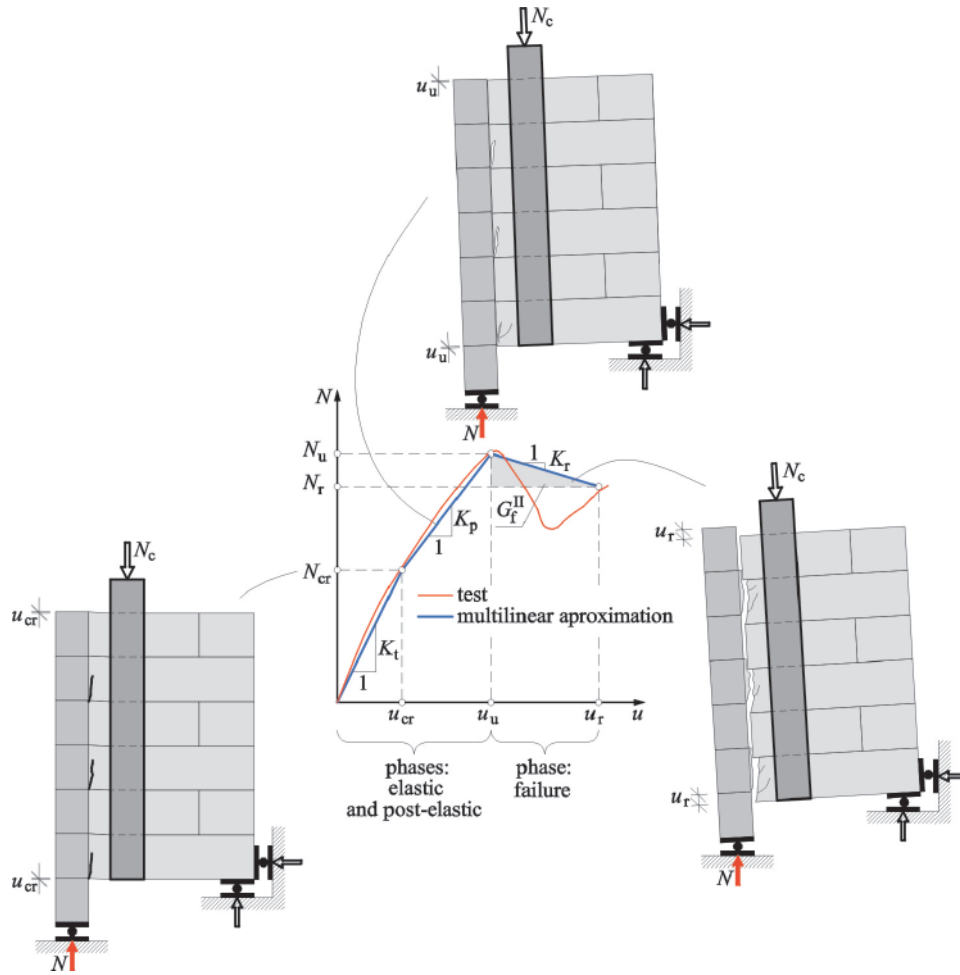


Figure 5. Linear approximation of joint's behaviour

Table 4. Comparison of test and calculation results

Joint model test			Calculation results		
Cracking force	Failure force	Residual force	Cracking force (7)	Failure force (9)	Residual force (11)
$N_{cr,mv}$ kN	$N_{u,mv}$ kN	$N_{r,mv}$ kN	N_{cr} kN	N_u kN	N_r kN
33.7	48.3	14.9	30.0	45.9	15.3
Cracking dis- placement	Failure dis- placement	Residual dis- placement	Cracking dis- placement (6)	Failure dis- placement (8)	Residual force (10)
$u_{cr,mv}$ mm	$u_{u,mv}$ mm	$u_{r,mv}$ mm	u_{cr} mm	u_u mm	u_r mm
0.10	0.24	6.32	0.09	0.24	4.27

In the failure phase, when a dry slip of the loosened walls occurred, the behaviour of the joint was modelled based on the standard tests according to PN-EN 1052-3:2004. In this type of tests measurements were made of relative displacements of two masonry elements joined with mortar. Fracture energy of the

joint, which according to continuum fracture mechanics allows describing the behaviour of a brittle material in the failure phase, was determined to be $G_f^{II} = 2.37 \cdot 10^{-4}$ MN/m [6]. Assuming that the fracture energy in a unit area of the joint G_f^{II} is equal to the one obtained in the test G_f^{II} , residual displace-

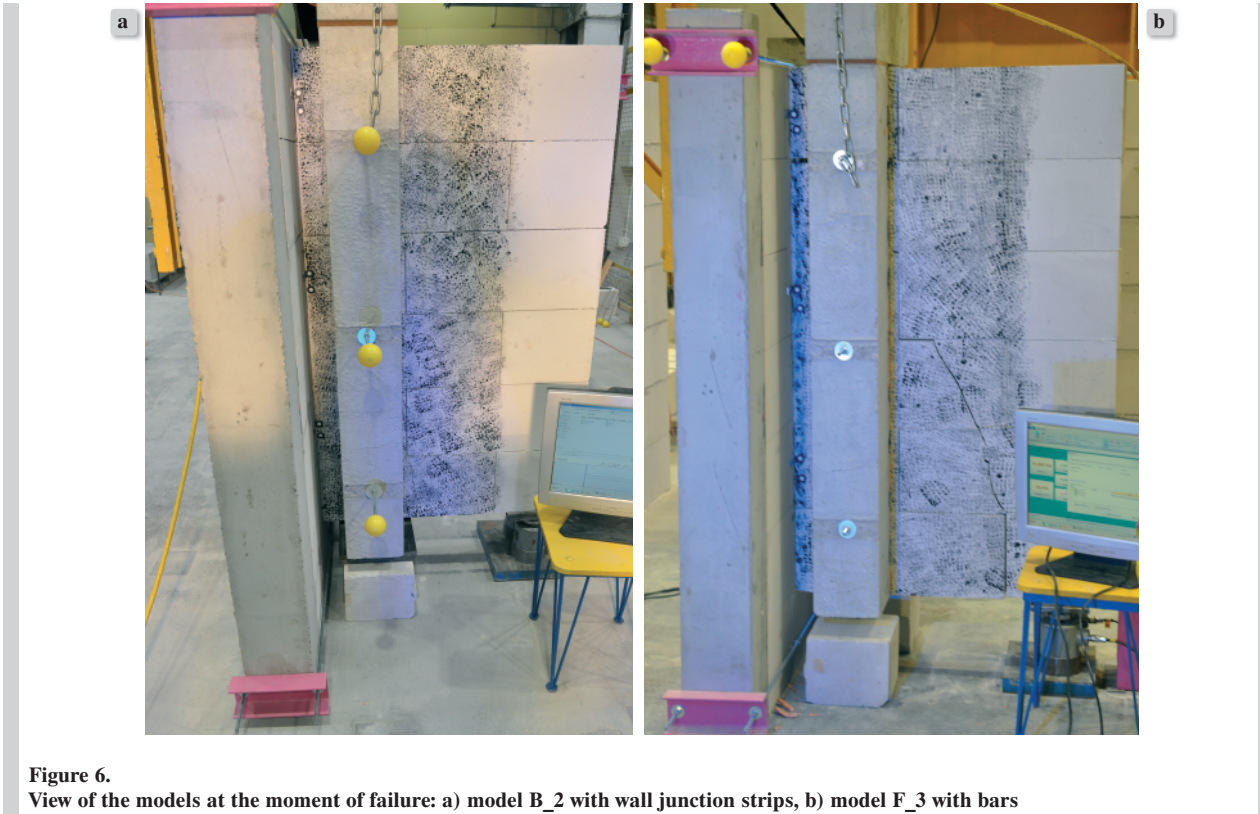


Figure 6. View of the models at the moment of failure: a) model B_2 with wall junction strips, b) model F_3 with bars

ments u_r were determined from the relation-ship:

$$G_f^{II} = G_f^{IIj} = \frac{1}{2} \frac{(N_u - N_r)(u_r - u_u)}{A} \Rightarrow u_r = u_u + \frac{2G_f^{II} A}{(N_u - N_r)} \quad (8)$$

where:

N_r – residua force equal to:

$$N_r = \gamma \tau_{u,RL} A, \quad (9)$$

where: $\gamma = 0.3$ – empirical coefficient.

Using the obtained semi-empirical relationships displacements were calculated; the results are collectively pre-sented in Table 4 and Fig. 5.

3.2. Reinforced models

In the models reinforced with steel connectors (**B** and **F** series) no cracking was observed as in unreinforced models. In the initial phase displacements between the joined walls were not visible. At a certain moment, a sudden, clearly noticeable increase in displacements occurred. However, it was still possible to further load the models until failure. Failure was sudden and caused by shear of the joint and visible vertical displacement (by approx. 17 mm) of the web wall – Fig. 7a, which settled on wooden protection. View

of the models at the mo-ment of failure is shown in Fig. 6. Failure of the models of **B** series with punched flat profiles was caused by plasticisation, bending of steel flat profiles in the joint (Fig. 7b). Thanks to the holes in the flat profile there was no slip of the connector in the mortar of bed joints: the mortar penetrating the holes was not sheared but acted as a dowel eliminating movement. The walls of **F** series, like the walls of **B** series, failed due to displacements of the loaded wall edge with relative to the unloaded edge. However, in this case, there was no plasticisation of the steel element. The steel bar was pressed into the concrete block under the shear force (Fig. 7c).

Phases of work of the element could be also present-ed in the diagrams of the load N – relative displacement u relationships of the joined walls (Fig. 8). Before cracking of the joint, which appeared under the load $N_{cr} = 12\text{--}24$ kN in **B** series models and 25–27 kN in **F** series models displacements were increasing almost proportion-ally; the phase was thus called an elastic phase. After cracking, in post-elastic phase displacements increased and forces decreased visibly to the values of $N_d = 9\text{--}17$ kN in **B** series models and 12–13 kN in **F** series models. In the post-elastic phase stiffness of the joint was reduced but the joint was still able to transfer loading.

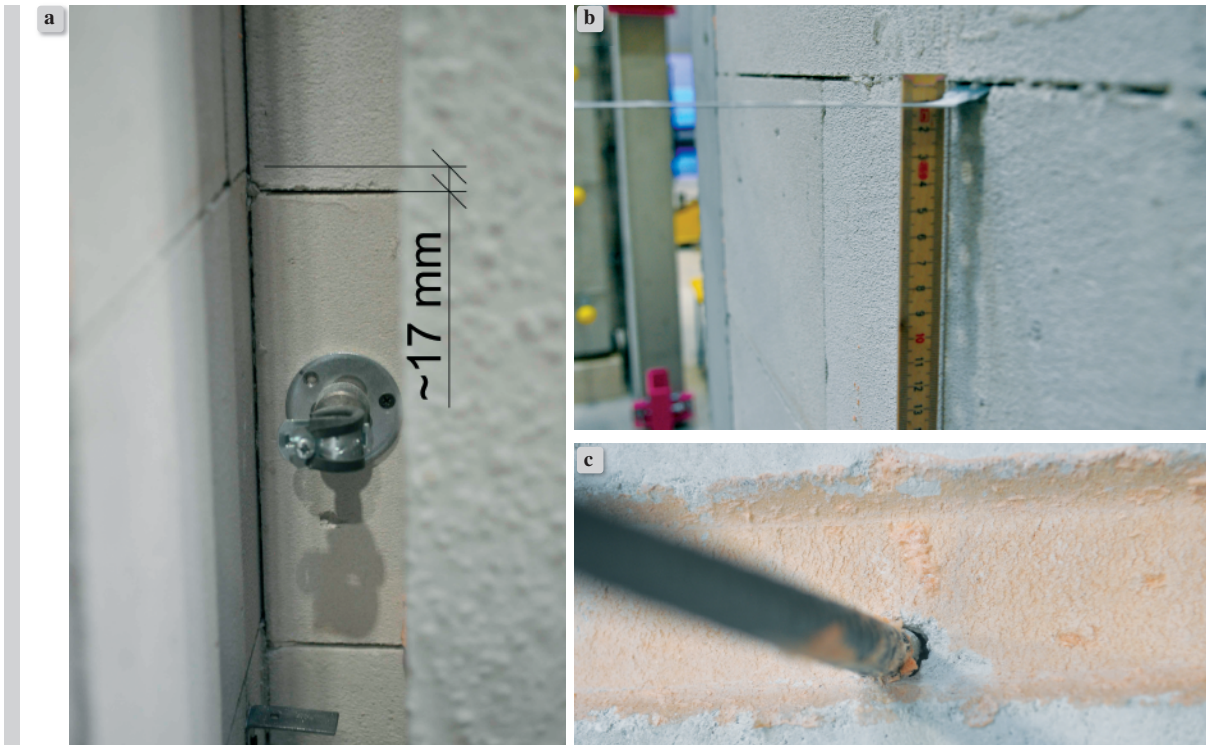


Figure 7. Failure of B and F series models a) view of a damaged model with dimensioned displacements between the bed joints in perpendicular walls (B_1) b) typical cambers in the wall junction strip flat profile within the joint (B_3) c) view of a bar joining the walls, pulled out after the test (F_2)

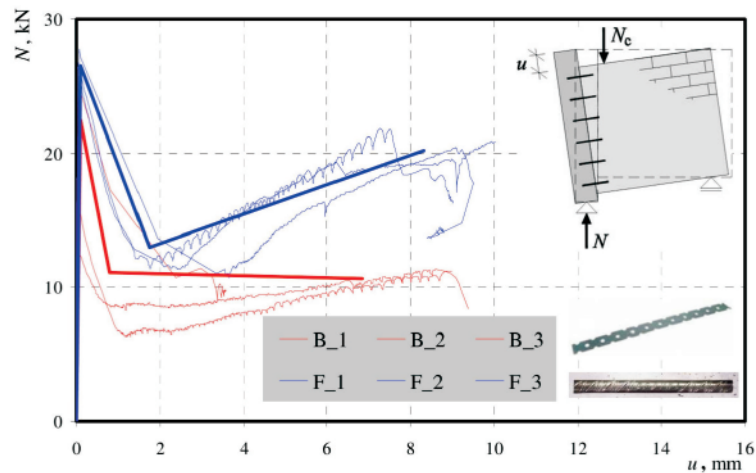


Figure 8. Relationship between the total force and mean relative displacement of the joint

The observed phases of work of the reinforced joint allowed to create an $N - u$ relationship of the joint of walls made of AAC composed of a sequence of straight lines (Fig. 9). Elastic phase was defined in the range of loads $0 - N_{cr}$, post-elastic phase in the range of loads $N_{cr} - N_d$, and failure phase in the range $N_d - N_u$.

The values of forces and accompanying displacements are collectively presented in Table 5, while linear approximation of the results is shown in Fig. 9. In each phase of work stiffnesses of the joints were determined according to the Eqs. (1–3) and collectively presented in Table 6.

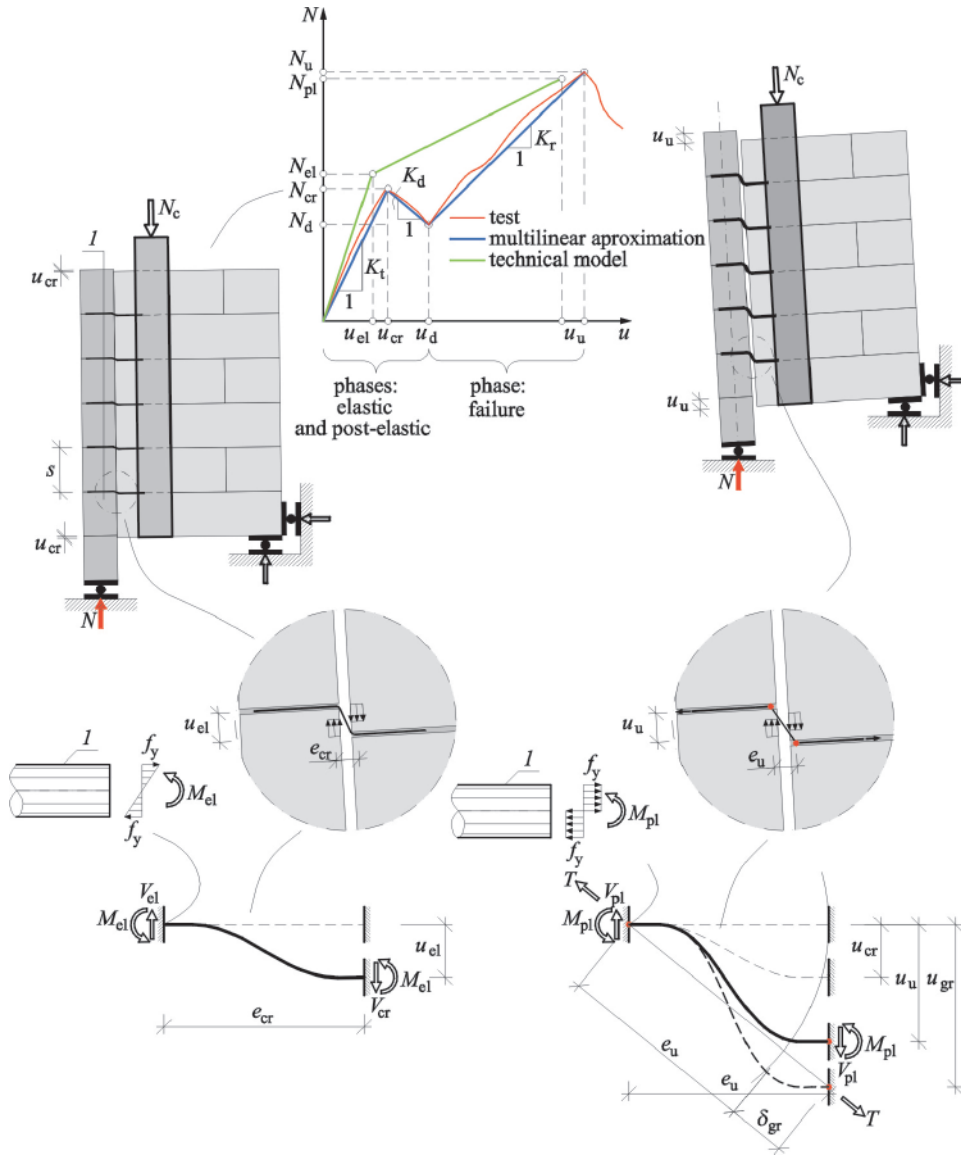


Figure 9. Linear approximation of work of reinforced joint ($I -$ connector)

Table 5. Test results

Model	Cracking force		Dowel force		Force at failure		Displacement at the moment of cracking		Dowel displacement		Displacement right before failure	
	N_{cr} kN	$N_{cr,mv}$ kN	N_d kN	$N_{d,mv}$ kN	N_u kN	$N_{u,mv}$ kN	u_{cr} mm	$u_{cr,mv}$ mm	u_d mm	$u_{d,mv}$ mm	u_u mm	$u_{u,mv}$ mm
B_1	24	17.6	17	11.1	10	10.6	0.12	0.09 (0.09t)	0.82	0.80	3.36	6.86 (6.86t)
B_2	16		7		11		0.05		1.06		8.60	
B_3	12		9		11		0.09		0.52		8.61	
F_1	25	26.5	13	13.0	21	20.2	0.12	0.09 (0.9φ)	1.29	1.75	6.96	8.31 (0.83φ)
F_2	28		14		20		0.07		1.94		9.17	
F_3	27		12		19		0.08		2.01		8.81	

Table 6.
Joint stiffness

Model	Elastic joint stiffness		Residual joint stiffness		Residual force	
	K_l MN/m	$K_{l,mv}$ MN/m	K_d MN/m	$K_{d,mv}$ MN/m	K_r MN/m	$K_{r,mv}$ MN/m
B_1	202	221	10	9	3	1
B_2	330		9		1	
B_3	132		7		0	
F_1	215	320	10	8	1	1
F_2	400		8		1	
F_3	344		8		1	

To theoretically represent phases of work of the joint it is necessary to perform auxiliary tests of the elements and conduct advanced FEM-based analyses of the models. However, to describe the behaviour of the joint some simplifications can be used derived from the literature of the subject [7, 8].

The following assumptions were made:

- walls are made of the Group 1 elements without holes with thin joints and unfilled head joints,
- thickness of bed joints allow assuring proper cover of the connectors,
- thickness of the stiffening wall is not bigger than the thickness of the transverse wall,
- there are two phases of work of the wall joint: elastic and failure,
 - Elastic phase in the range of loads $0 - N_{el}$ and displacements $0 - u_{el}$,
 - Failure phase in the range of loads $N_{el} - N_r$ and displacements $u_{el} - u_u$,

In which the relationships between the load and displacement $N - u$ are approximated with straight lines.

- in all phases of work shear load is transferred by the connectors acting as bars fixed at both ends in the bed joints mortar,
- the value of force causing displacement u is expressed with the following relationship:

$$V = \frac{12EI}{e^3}u, \quad (10)$$

while the corresponding moment is equal to:

$$M = \frac{6EI}{e^2}u, \quad (11)$$

where:

EI – flexural stiffness of the connector, u – relative displacement of the connector's ends, e – the effective length of the connector (distance between the fixation points).

g) the model of the reinforced joint can be used under the following conditions:

- In the elastic phase, when equations of the displacement method are used, the influence of normal forces on the elongation of the bar is neglected and vertical displacement u is small with respect to the connector's length e , $u_{el,gr} \leq 0.05e$ was assumed,
- Relative displacements determined at the moment of plastic hinges formation in the connectors satisfy the conditions: $u \leq u_{gr}$ and $u \leq u_{gr,y}$ (u_{gr} – displacements causing pulling out of the connector from the wall, $u_{gr,y}$ – displacement causing yielding of the connector),
- Length of the connector in the limit state must satisfy the conditions: $e_{pl} \leq e_{gr} = l$ (l – initial connector's length).

Stresses in the outermost fibres of the connector fixed in bed joints increase proportionally to the displacement u . At a certain level of displacement u_{el} these stresses reach plasticity limit and bending moment, as well as transverse force, are described with the following formulas:

$$M_{el} = f_y W_{el} = \frac{6EI}{e_{el}^2} u_{el}, \quad V_{el} = \frac{2M_{el}}{e_{el}}. \quad (12)$$

where: W_{el} – elastic bending index of the connector's cross-section, f_y – yield strength of the connector's steel, e_{el} – connector's length in the elastic phase.

With an increase of relative displacement of the connector's ends the whole cross-section of the connector yields and the reactions at the end are equal to:

$$M_{pl} = f_y W_{pl} = \frac{6EI}{e_{pl}^2} u_{pl}, \quad V_{pl} = \frac{2M_{pl}}{e_{pl}}, \quad (13)$$

where: W_{pl} – plastic bending index of the connector's cross-section, f_y – yield strength of the connector's steel, e_{pl} – connector's length in plastic phase.

Apart from the material parameters such as plasticity limit of elastic modulus, in Eqs. (12) and (13) there appear also the lengths of connectors e_{el} and e_{pl} . In [7] it has been experimentally shown that in flat-profile connectors the lengths of the connectors were equal to $(1.6-2.5)t$ while for the bar connectors to 0.9ϕ . Following [8], after transformation of Eqs. (12) and (13) and by considering forces obtained in each phase of the work, the lengths of the connectors were calculated with the following formulas:

$$e_{cr} = \frac{2nf_y W_{el}}{N_{cr,mv}}, e_d = \frac{2nf_y W_{el}}{N_{d,mv}}, e_u = \frac{2nf_y W_{pl}}{N_{u,mv}}, \quad (14)$$

The obtained results are collectively presented in Table 7.

Table 7.
Lengths of connectors determined based on the condition of forces acting in the joint

Type of connector	Elastic phase	Post-elastic phase	Failure phase	Mean value
	$e_{cr,mv}$ mm	$e_{d,mv}$ mm	$e_{u,mv}$ mm	
B	0.35 (0.35t)	0.56 (0.56t)	0.87 (0.87t)	0.59 (0.59t)
F	23.8 (2.4φ)	48.6 (4.9φ)	53.0 (5.3φ)	41.8 (4.18φ)

The connectors lengths e were noticeably different in each phase of work. In case of B-type connectors, the lengths did not exceed $0.59t$ while for F-type connectors they were equal to around 4.18ϕ . In both cases, the greatest lengths of connectors were obtained in the failure phase and they were equal to around $0.87t$ for flat profiles and 5.3ϕ for bars. Therefore, the obtained results deviate from the ones presented in [7], because in the case of flat-profile connectors the obtained lengths were about 50% higher while in the case of bar connectors significantly higher.

Assuming that the length of the connector is equal to e , the values of bending moments causing yielding of the outermost fibres as well as total yielding of the connector, can be determined. The values of forces and accompanying displacements were determined with the formulas:

$$N_{el} = \sum V_{el} = \frac{2nf_y W_{el}}{e}, u_{el} = \frac{f_y W_{el} e^2}{6EI}, \quad (15)$$

$$N_{pl} = \sum V_{pl} = \frac{2nf_y W_{pl}}{e}, u_{pl} = \frac{f_y W_{pl} e^2}{6EI}. \quad (16)$$

where: V_{el} – force causing yielding of the outermost fibres of a single connector, V_{pl} – force causing yield-

ing of the whole cross-section of a single connector, e – mean connector’s length equal to $0.59t$ for punched flat pro-files and 4.18ϕ for bars.

The obtained results of failure forces are collectively presented in Table 8.

As a result of the applied procedure for the determination of the connectors length, the obtained values of forces inducing yielding stresses in the outermost fibres of the connectors were smaller than experimentally-determined cracking forces. The difference was equal to 69–76%. On the other hand, in the phase of complete yielding undesirable overestimation of load-bearing capacity was obtained as the calculated forces were by around 21%–32% higher than the forces obtained in the tests. The obtained displacements results, which were significantly smaller than the experimental ones require also some comment. It was assumed that the connectors have ends fixed in either bed joints or masonry elements. As shown in Fig. 9 under large vertical displacements occurring in the failure phase horizontal displacements δ_u should not be neglected as it was done in elastic phase. Under full fixation of connectors in the wall horizontal displacements can induce important tensioning of the connector (force T in Fig. 9) while in reality the bond between mortar and connectors is broken and connectors slip from the wall. The effect of horizontal displacements can be additionally magnified by constructional imperfections (voids within the connectors zone) which are hard to eliminate. Visual inspection of B-type connectors indicated irreversible deformations (Fig. 7) and the distance between plastic hinges e was visibly larger than calculated and shown in Table 7. In the case of F-type connectors, no characteristic irreversible deformations were observed but spalling of masonry element under the local pressure was noticed.

The ultimate value of vertical displacement can be determined assuming that at vertical displacement of the connector the force T is equilibrated by the load-

Table 8.
Calculated lengths of connectors

Type of connector	Displacements		Forces		$\frac{N_{cr,mv}}{N_{el}}$	$\frac{N_{u,mv}}{N_{pl}}$	Ultimate displacements	
	Elastic phase	Failure phase	Elastic phase	Failure phase			Assumptions of the method	Condition of the connector’s rapture (21)
	u_{el} mm	u_{pl} mm	N_{el} kN	N_{pl} kN			$u_{el,gr}$ mm	$u_{gr,y}$ mm
B	$2.48 \cdot 10^{-4}$	$3.72 \cdot 10^{-4}$	10.4	15.6	1.69	0.68	0.02 mm (0.02t)	0.04 (0.04t)
F	$1.64 \cdot 10^{-1}$	$2.78 \cdot 10^{-1}$	15.1	25.6	1.76	0.79	1.19 mm (0.12φ)	3.14 (0.31φ)

bearing capacity of the connector anchored in the bed joint's mortar. The horizontal component of the force results from elongation of the connector δ_{gr} caused by vertical displacement u_{gr} . From these simple geometrical relationships, it can be concluded that:

$$\delta_{gr} = \sqrt{e_u^2 + u_{gr}^2} - e_u, \quad (17)$$

and a corresponding force is equal to:

$$T = \frac{E_s A}{e_u} \delta_{gr} \rightarrow \frac{E_s A}{e_u} \left(\sqrt{e_u^2 + u_{gr}^2} - e_u \right). \quad (18)$$

The force causing elongation of the connectors should be equilibrated by the adhesion force T_{bond} between mortar and the connector, which can be determined as:

$$T_{bond} = f_{bond} l_b O_b, \quad (19)$$

where:

f_{bond} – ultimate bond stress of mortar to the connector determined experimentally,

l_b – the active length of the connector in bed joint reduced by half of the distance between plastic hinges,

O_b – the perimeter of the active part of the connector in bed joint.

Finally, the ultimate vertical displacement can be written in the following form:

$$T \leq T_{bond} \rightarrow \frac{E_s A}{e_u} \left(\sqrt{e_u^2 + u_{gr}^2} - e_u \right) \leq f_{bond} l_b O_b \rightarrow$$

$$\rightarrow u_{gr} = e_u \sqrt{\left(\frac{f_{bond} l_b O_b}{E_s A} + 1 \right)^2} - 1. \quad (20)$$

Additionally, a condition must be taken into account of yielding of the connector's cross-section due to elongation, then the additional condition can be expressed as:

$$T \leq f_y A \rightarrow \frac{E_s A}{e_u} \left(\sqrt{e_u^2 + u_{gr,y}^2} - e_u \right) \leq f_y A \rightarrow$$

$$\rightarrow u_{gr,y} = e_u \sqrt{\left(\frac{f_y}{E_s} + 1 \right)^2} - 1. \quad (21)$$

The ultimate vertical displacements expressed with Eqs. (20) and (21) depend on the value e_u , so on the length of the connectors and the ultimate bond

stresses f_{bond} . Both values must be determined experimentally with the use of small testing models allowing to eliminate the factors present in the wall models. For example, the ultimate displacements of the connector determined with Eq. (21), in which the value of e_u was assumed to be equal to $0.59t$ and 4.18ϕ , obtained at the moment of yielding (Table 7) were equal to, respectively: $0.04t = 0.04\text{ mm}$ (B-type connector) and $0.31\phi = 3.1\text{ mm}$ (P-type connector) (Table 8). One can think that the calculated ultimate displacements are too safe as the joints were characterised with significantly higher deformability. Moreover, no permanent elongation of the connectors (signifying yielding) was observed.

Relatively scarce research material allows determining the displacements and stiffnesses of joints currently only based on the results of experimental tests results. Taking into consideration the results of connectors displacements the substitute lengths of the connectors were determined from the formulas:

$$e_{cr,u} = \sqrt{\frac{6u_{cr,mv}EI}{f_y W_{el}}}, \quad (22)$$

$$e_{u,u} = \sqrt{\frac{6u_{u,mv}EI}{f_y W_{pl}}}, \quad (23)$$

The obtained results are collectively presented in Table 9.

Table 9.
Lengths of connectors determined from the conditions of displacements

Type of connector	Elastic phase	Failure phase	Limit length of the connector
	$e_{el,u}$ mm	$e_{pl,u}$ mm	e_{gr} mm
B	11.2 (11t)	80.5 (80t)	300 t
F	30.7 (3.1 φ)	228.5 (22.9 φ)	30 φ

Of course, the equivalent lengths of connectors do not have a physical meaning because they were determined for a hypothetical state of yielding of the outermost fibres or entire cross-section. In the B-type connectors, the lengths of around (11–80)t were obtained while for determination of force a mean length of a connector was equal to 0.22t. In case of F-type connectors the substitute lengths of connectors for determination of displacements were equal to (30–228)φ, so much more than the lengths allowing to determine the values of V_{el} and V_{pl} forces in which the length of 1.43φ was used.

Summarizing, the values of forces and displacements, as well as the stiffnesses of the joint, can be determined using the engineering models of the joint with the following formulas:

- Elastic phase – B-type connector:

$$N_{el} = \xi \frac{2nf_y W_{el}}{0,59t}, \quad (24)$$

$\xi = 1.7$ – empirical coefficient for determination of the value of force causing yielding of the outermost fibres of the connector,

$$u_{el} = \frac{f_y W_{el} (11t)^2}{6EI}, \quad (25)$$

$$K_t = \xi \frac{12nEI}{0,59t(11t)^2}. \quad (26)$$

- Post-elastic phase – B-type connector:

$$N_{pl} = \xi_1 \frac{2nf_y W_{pl}}{0,59t}, \quad (27)$$

$\xi_1 = 0.65$ – empirical coefficient for determination of the value of force causing yielding of the whole cross-section of the connector,

$$u_{pl} = \frac{f_y W_{pl} (80t)^2}{6EI}, \quad (28)$$

$$K_r = \frac{N_{pl} - N_{el}}{u_{pl} - u_{el}}, \quad (29)$$

- Elastic phase – F-type connector:

$$N_{el} = \xi \frac{2nf_y W_{el}}{4,18\phi}, \quad (30)$$

$$u_{el} = \frac{f_y W_{el} (30\phi)^2}{6EI}, \quad (31)$$

$$K_t = \xi \frac{12nEI}{4,18\phi(30\phi)^2}, \quad (32)$$

- Post-elastic phase – F-type connector:

$$N_{pl} = \xi_1 \frac{2nf_y W_{pl}}{4,18\phi}, \quad (33)$$

$$u_{pl} = \frac{f_y W_{pl} (22,9t)^2}{6EI}, \quad (34)$$

$$K_r = \frac{N_{pl} - N_{el}}{u_{pl} - u_{el}}, \quad (35)$$

The values of empirical coefficients ξ and ξ_1 used in the equations were determined by comparison between empirical values and the values calculated acc. to Table 8 assuming equal values in case of B- and P-type connectors. The values of forces and displacement calculated according to the above equations are shown in Fig. 10.

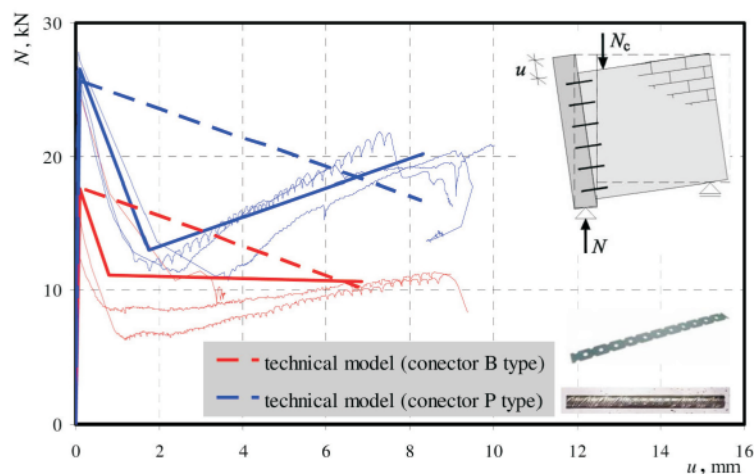


Figure 10. Comparison of test results with the calculation results according to the engineering model

4. SUMMARY

The presented tests are a part of the research performed currently at the Laboratory of Civil Engineering Faculty of the Silesian University of Technology in the topic of joints of walls made of AAC blocks. Hereafter are presented only three models with traditional masonry bond.

The process of damage and development of cracking in the wall with masonry bond was progressing in stages and was relatively smooth. Before failure, visible cracking developed within the joint. Individual phases of work were defined based on which an empirical method was proposed for the determination of forces and displacements in wall joints using the results of simple standard tests. With such an approach satisfactory compliance was achieved. The paper presents also test results of joints with steel connectors: wall junction strip (B models) and bars (F models). Analogically as in case of unreinforced walls, the phases of work of the joints were identified and de-scribed. Base on the well-known relationships, an engineering approach was proposed for determination of the values of cracking and maximum forces in the joint.

Future works should include testing of additional model elements for the statistical definition of empirical pa-rameters of the models as well as the parameters defining anchorage of the connectors in bed joints or in the masonry wall. FEM-based analyses are also necessary for proper characterization of joints behaviour and mostly for determination of their realistic length – e . The final model should also take into consideration the softening phase in the joint and should sufficiently precisely estimate the values of N_{cr} , N_d and N_u forces as well as corresponding displacements.

ACKNOWLEDGEMENTS

The authors would like to thank the companies Solbet Sp. z o.o. and NOVA Sp. z o.o. for their valuable tips and supply of materials (masonry units, mortar and steel connectors) used to build the test models and perform the tests.

REFERENCES

- [1] Galman, I., & Jasiński, R. (2018). Joints in masonry walls. 6th International Conference on Autoclaved Aerated Concrete. 4–6 September 2018, University Potsdam, Germany. Ce/Papers Ernst & Sohn, 339–346. <https://doi.org/10.1002/cepa.855>.
- [2] PN-EN 1052-1:2000 Methods of tests for masonry. Part 1: Determination of Compression Strength (in Polish).
- [3] PN-EN 1052-3:2004 Methods of tests for masonry. Part 3: Determination of Initial Shear Strength (in Polish).
- [4] ASTM E519-81 Standard Test Method for Diagonal Tension (Shear) of Masonry Assemblages.
- [5] Galman, I., & Jasiński, R. (2018). An Attempt to Describe the Mechanism of Work of Masonry Joints, 3rd World Multidisciplinary Civil Engineering – Architecture – Urban Planning Symposium. 18–22 June 2018, Czech Republic, Prague.
- [6] Jasiński, R. (2017) Research and modeling of masonry shear walls (PhD DSc thesis, Silesian University of Technology). Poland, Gliwice (in Polish).
- [7] Simudic, G., & Page, A.,W. (1996). Australian developments in the use of walls of geometric section. 7th North American Masonry Conference. University of Notre Dame-South Bend, Indiana, USA, 2–5 June 1996. Vol.2, 1007–1018.
- [8] Phipps, M., E., & Montague, T.,I. (1996). The behaviour and design of steel shear connectors in plain and prestressed masonry. 7th North American Masonry Conference. University of Notre Dame-South Bend, Indiana, USA, 2–5 June 1996. Vol.2, 789–798.